

## Synchrotron X-Ray Fluorescence Nanoprobe Reveals Target Sites for Organo-Osmium Complex in Human Ovarian Cancer Cells

Sanchez-cano, Carlos; Romero-canelón, Isolda; Yang, Yang; Hands-Portman, Ian J.; Bohic, Sylvain; Cloetens, Peter; Sadler, Peter J.

DOI:

[10.1002/chem.201605911](https://doi.org/10.1002/chem.201605911)

License:

Creative Commons: Attribution (CC BY)

*Document Version*

Publisher's PDF, also known as Version of record

*Citation for published version (Harvard):*

Sanchez-cano, C, Romero-canelón, I, Yang, Y, Hands-Portman, IJ, Bohic, S, Cloetens, P & Sadler, PJ 2017, 'Synchrotron X-Ray Fluorescence Nanoprobe Reveals Target Sites for Organo-Osmium Complex in Human Ovarian Cancer Cells', *Chemistry: A European Journal*, vol. 23, no. 11, pp. 2512-2516.  
<https://doi.org/10.1002/chem.201605911>

[Link to publication on Research at Birmingham portal](#)

### **Publisher Rights Statement:**

C. Sanchez-Cano, I. Romero-Canelón, Y. Yang, I. J. Hands-Portman, S. Bohic, P. Cloetens, P. J. Sadler, *Chem. Eur. J.* 2017, 23, 2512

Published in *Chemistry - A European Journal* on 24/12/2016

DOI: 10.1002/chem.201605911

### **General rights**

Unless a licence is specified above, all rights (including copyright and moral rights) in this document are retained by the authors and/or the copyright holders. The express permission of the copyright holder must be obtained for any use of this material other than for purposes permitted by law.

- Users may freely distribute the URL that is used to identify this publication.
- Users may download and/or print one copy of the publication from the University of Birmingham research portal for the purpose of private study or non-commercial research.
- User may use extracts from the document in line with the concept of 'fair dealing' under the Copyright, Designs and Patents Act 1988 (?)
- Users may not further distribute the material nor use it for the purposes of commercial gain.

Where a licence is displayed above, please note the terms and conditions of the licence govern your use of this document.

When citing, please reference the published version.

### **Take down policy**

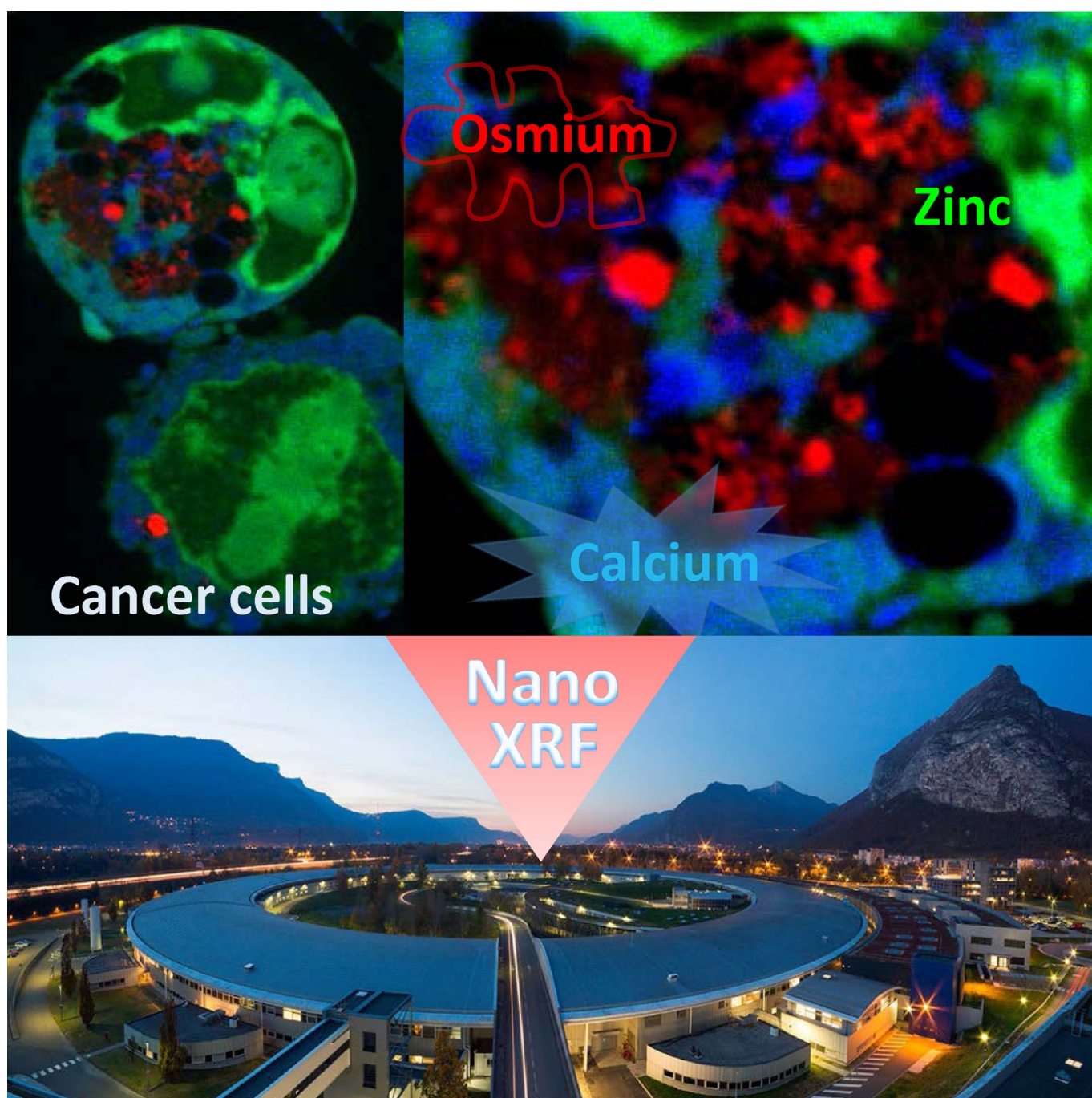
While the University of Birmingham exercises care and attention in making items available there are rare occasions when an item has been uploaded in error or has been deemed to be commercially or otherwise sensitive.

If you believe that this is the case for this document, please contact [UBIRA@lists.bham.ac.uk](mailto:UBIRA@lists.bham.ac.uk) providing details and we will remove access to the work immediately and investigate.

## ■ Organometallic Complexes

**Synchrotron X-Ray Fluorescence Nanoprobe Reveals Target Sites for Organo-Osmium Complex in Human Ovarian Cancer Cells**

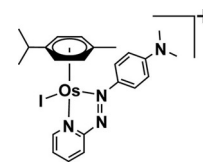
Carlos Sanchez-Cano,<sup>\*,[a]</sup> Isolda Romero-Canelón,<sup>[a]</sup> Yang Yang,<sup>[b]</sup> Ian J. Hands-Portman,<sup>[d]</sup> Sylvain Bohic,<sup>[b, c]</sup> Peter Cloetens,<sup>\*,[b]</sup> and Peter J. Sadler<sup>\*,[a]</sup>



**Abstract:** A variety of transition metal complexes exhibit anticancer activity, but their target sites in cells need to be identified and mechanisms of action elucidated. Here, it was found that the sub-cellular distribution of  $[\text{Os}(\eta^6\text{-}p\text{-cym})(\text{Azpy-NMe}_2)]^+$  ( $p\text{-cym} = p\text{-cymene}$ ,  $\text{Azpy-NMe}_2 = 2\text{-}(p\text{-[dimethylamino]phenylazo)pyridine}$  (1), a promising drug candidate, can be mapped in human ovarian cancer cells at pharmacological concentrations using a synchrotron X-ray fluorescence nanoprobe (SXRFN). SXRFN data for Os, Zn, Ca, and P, as well as TEM and ICP analysis of mitochondrial fractions suggest localization of Os in mitochondria and not in the nucleus, accompanied by mobilization of Ca from the endoplasmic reticulum, a signaling event for cell death. These data are consistent with the ability of 1 to induce rapid bursts of reactive oxygen species and especially superoxide formed in the first step of  $\text{O}_2$  reduction in mitochondria. Such metabolic targeting differs from the action of Pt drugs, offering promise for combating Pt resistance, which is a current clinical problem.

The most widely used drugs in cancer chemotherapy are platinum complexes, cisplatin, carboplatin, and oxaliplatin. Despite their success, resistance to platinum is now a clinical problem, as is the need to reduce side-effects and extend treatment to a wider range of cancers.<sup>[1]</sup> These challenges might be remedied by complexes of other second and third-row transition metals if they have different mechanisms of action from platinum, for instance by targeting sites other than nuclear DNA or by causing distinctly different lesions on DNA. Recently, organometallic half-sandwich  $\text{Os}^{\text{II}}$  arene complexes have shown promise.<sup>[2]</sup> Using phenotypic screening, we discovered high ac-

tivity within a series of  $\text{Os}^{\text{II}}$  arene azopyridine complexes. For example,  $[\text{Os}(\eta^6\text{-}p\text{-cym})(\text{Azpy-NMe}_2)]\text{PF}_6$  (where  $p\text{-cym} = p\text{-cymene}$  and  $\text{Azpy-NMe}_2 = 2\text{-}(p\text{-[dimethylamino]phenylazo)pyridine}$  (1, Scheme 1) is 49× more potent than cisplatin towards a range of 809 cancer cell lines, and not cross-resistant with cisplatin or oxaliplatin.<sup>[3]</sup> Identifying the target sites for metallodrugs in cells is a challenging task, but is assisted for precious metals by their normal absence.



**Scheme 1.** Structure of  $[\text{Os}(\eta^6\text{-}p\text{-cym})(\text{Azpy-NMe}_2)]^+$  (1).

Two promising techniques for characterizing the sub-cellular distribution of metallodrugs are secondary ion mass spectrometry (SIMS) and synchrotron-based X-ray fluorescence (SXRF). Importantly, these high resolution multi-element analysis techniques allow simultaneous mapping of essential elements such as P and Zn in cells. The recent development of nanoscale probing for SIMS (NanoSIMS) has allowed cellular organelles to be analyzed. For example, Pt from cisplatin and Triplatin C has been detected by NanoSIMS (maximum resolution of  $80 \times 80 \text{ nm}^2$ ) in the nucleolus of MCF7 cells,<sup>[4]</sup> whereas Ru from anti-metastatic organometallic complexes has been found in membranes or intercellular junctions,<sup>[5]</sup> and gold phosphine anti-cancer complexes in the nucleus and cytoplasm.<sup>[6]</sup> However, NanoSIMS offers low sensitivity towards second and third-row transition metals (due to low ionization yield),<sup>[7]</sup> and requires treatment of cells with elevated drug concentrations.

SXRF has also been used to investigate anticancer metal compounds in vivo and in vitro. Thus, the cellular distribution of Pt, Gd, Ru, Se, and As metallodrugs<sup>[8]</sup> and Nb, Co, Ti, and V metallocenes has been explored by micro-SXRF.<sup>[9]</sup> Pt-based DNA-intercalators have been found concentrated in the nuclei of cells, whereas cisplatin is evenly distributed throughout the cell.<sup>[8c]</sup> SXRF experiments have suggested that Gd complexes carrying triphenylphosphonium substituents can localize in the mitochondria of cells (although mitochondria were not distinctly resolved in the maps acquired)<sup>[8h]</sup> and that Zn plays an important role in the resistance to cisplatin.<sup>[8b]</sup> However, the spatial resolution achieved previously by micro-SXRF (from  $0.2 \times 0.2$  to  $1.5 \times 1.5 \mu\text{m}^2$  beam size) made it difficult to assess accurately the subcellular localization of metals, especially within small organelles with sizes  $\leq 1 \mu\text{m}$  (which cannot be resolved). It also usually required treatment of cells with extremely high concentrations of drug ( $> 100 \mu\text{M}$ ), although more relevant concentrations have been used in some experiments ( $1\text{--}20 \mu\text{M}$ ).<sup>[8b,d,i,j]</sup>

Newly designed SXRF nanoprobe (SXRFN) now allow acquisition of elemental maps with  $100 \times 100 \text{ nm}^2$  resolution.<sup>[10]</sup> For example, SXRFN analysis revealed the localization of a Ru antimalarial drug within the digestive vacuole of *Plasmodium falciparum*-infected erythrocytes ( $80 \times 80 \text{ nm}^2$  spot size; scanned using a  $100 \times 100 \text{ nm}^2$  step size).<sup>[10a]</sup>

Here we use the new nano-imaging beamline ID16A at the ESRF, capable of focussing the hard X-ray beam size down to  $27 \times 37 \text{ nm}^2$ . This represents a significant reduction in the surface of the spot size compared to previous use, and provides

[a] Dr. C. Sanchez-Cano, Dr. I. Romero-Canelón, Prof. Dr. P. J. Sadler  
Department of Chemistry  
University of Warwick  
Coventry, CV4 7AL (UK)  
E-mail: c.sanchez@warwick.ac.uk  
p.j.sadler@warwick.ac.uk

[b] Dr. Y. Yang, Dr. S. Bohic, Dr. P. Cloetens  
ID16A beamline, ESRF, The European Synchrotron  
71 Avenue des Martyrs, 3800 Grenoble (France)  
E-mail: cloetens@esrf.fr

[c] Dr. S. Bohic  
Inserm, U836, equipe 6  
"Rayonnement synchrotron et recherches medicales", Grenoble  
Institut des Neurosciences  
38054 Grenoble (France)

[d] I. J. Hands-Portman  
School of Life Sciences, University of Warwick  
Coventry, CV4 7AL (UK)

Supporting information and ORCID identification numbers of the authors for this article can be found under:  
<http://dx.doi.org/10.1002/chem.201605911>.

© 2017 The Authors. Published by Wiley-VCH Verlag GmbH & Co. KGaA. This is an open access article under the terms of the Creative Commons Attribution License, which permits use, distribution and reproduction in any medium, provided the original work is properly cited.



sufficient resolution for the study of sub-cellular organelles. Furthermore, the unique flux of about  $4 \times 10^{11}$  photons per second available at ID16A allows detection of organometallic anticancer complexes at medically relevant concentrations in thin cellular sections.<sup>[11]</sup>

We acquired SXRF elemental maps for A2870 human ovarian carcinoma cells treated with **1**, using an excitation energy of 17.05 keV and a beam-size of  $27 \times 37 \text{ nm}^2$  (H $\times$ V) in all experiments. Samples were scanned using step sizes of  $50 \times 50 \text{ nm}^2$  or  $20 \times 20 \text{ nm}^2$  (the smallest reported for biological samples). This sampling is consistent with the resolution offered by the focus ( $\approx 2$  pixel elements per resolution element). Sample preparation is important for the preservation of biologically relevant elements in adherent mammalian cells. Initial maps showed that paraformaldehyde (PFA) preserved the structure of A2870 cells better than methanol fixation (Figure S1 in the Supporting Information). Interestingly, recent reports suggest that PFA fixation is also not ideal; although it maintains the localization of Zn, it leads to increased elemental leaching when compared to PFA + glutaraldehyde fixation or vitrification followed by freeze drying.<sup>[12]</sup> The appropriate level of exposure of cells to **1** so as to achieve intracellular SXRFN detection of Os was optimized using ICP-MS (Table S1). As a result, Os maps for whole A2870 cells treated for 24 h with biologically relevant concentrations of **1** ( $\text{IC}_{50}$ :  $0.16 \mu\text{M}$  or  $6 \times \text{IC}_{50}$ :  $1 \mu\text{M}$ ) and fixed with 2% PFA were acquired using a  $50 \times 50 \text{ nm}^2$  scan step size and 50 ms dwell time (Figure 1 and Figure S2 in the Supporting Information). These maps confirmed that **1** is detectable even at drug concentrations as low as 160 nM. SXRFN maps acquired from 500 nm-thick sections of Epon-embedded cells ( $1 \mu\text{M}$  **1**, 24 h; raster scan step sizes  $50 \times 50 \text{ nm}^2$  or  $20 \times 20 \text{ nm}^2$ ; 50 ms dwell time) showed that **1** readily penetrates cells (Figures 2 and 3 and Figures S4 and S5 in the Supporting Information). Osmium localization does not overlap with Zn and there is only marginal overlap with P (Figures 2 and 3; confirmed by co-localization analysis, Figures S6 and S7). Zinc and P are found mostly in cell nuclei (e.g., as Zn-finger proteins).<sup>[13]</sup> This indicates that **1** is not localized in the nuclei of treated cells, and suggests that DNA is not a major target for **1**.

Interestingly, Os from **1** appeared to be significantly compartmentalized within small organelles in cells, concentrated in small elliptical areas approximately 270 nm in length (Figures 1–4 and Figure S8 in the Supporting Information). SXRFN maps of 3T3 cells with mitochondria labeled with gold have shown similar patterns.<sup>[10c]</sup> Additionally, TEM images showed the existence of dark particles of around 350 nm in length in treated and 400 nm in untreated cells (Figure S9). These elliptical particles are similar in size and shape to the mitochondria of fast-growing tumor cells such as A2870, and to other organelles such as endosomes, lysosomes, and peroxisomes. Attempts to identify organelle localization of **1** using Os–Au co-localization in SXRFN maps with antibody-conjugated nano-gold<sup>TM[14]</sup> were unsuccessful due to the low efficiency of antibody labeling (data not shown).

Supporting evidence for localization of Os in mitochondria was obtained by isolating mitochondrial fractions from A2870

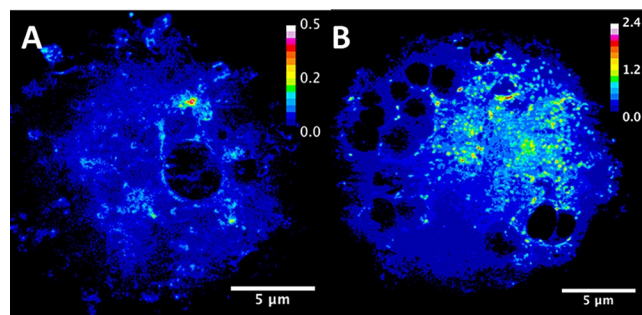


**Figure 1.** XRF maps of Os in whole A2870 ovarian cancer cells treated for 24 h with A)  $\text{IC}_{50}$  concentration of **1**; B)  $1 \mu\text{M}$  **1**. Raster scan:  $50 \times 50 \text{ nm}^2$  step size, 50 ms dwell time. Scale bar 5  $\mu\text{m}$ . Calibration bar in  $\text{ng mm}^{-2}$ .

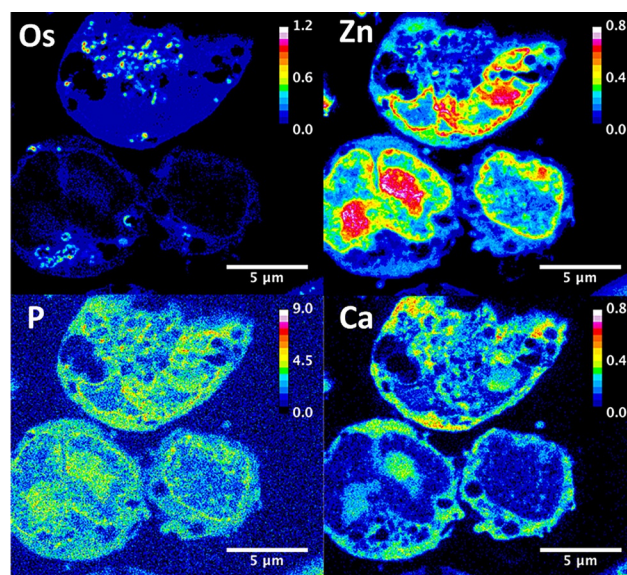


**Figure 2.** XRF maps of a 500 nm thick section of A2870 cells treated for 24 h with  $1 \mu\text{M}$  **1** showing the cellular distribution of Os, Zn, P, and Ca. Raster scan:  $50 \times 50 \text{ nm}^2$  step size, 50 ms dwell time. Scale bar 2  $\mu\text{m}$ . Calibration bar in  $\text{ng mm}^{-2}$ .

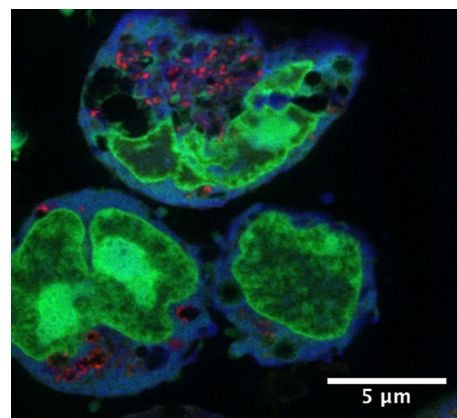


**Figure 3.** Co-localization XRF map of a 500 nm-thick section of A2870 cells treated for 24 h with  $1 \mu\text{M}$  **1** showing the cellular distribution of Os (red), Zn (green), and Ca (blue). Raster scan:  $50 \times 50 \text{ nm}^2$  step size, 50 ms dwell time. Scale bar 5  $\mu\text{m}$ .

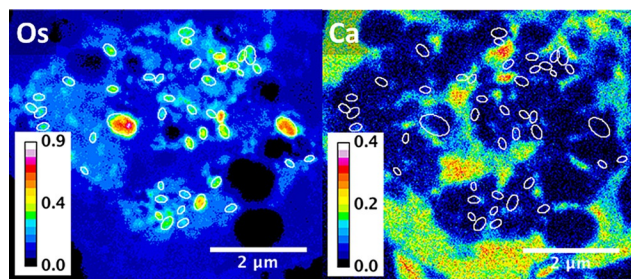


**Figure 4.** XRF maps of a 500 nm-thick section of A2780 cells treated for 24 h with  $1 \mu\text{M}$  **1** showing the cellular distribution of Os and Ca. Raster scan:  $20 \times 20 \text{ nm}^2$  step size, 50 ms dwell time. White ellipses show the absence of Ca in areas with high density of Os. Scale bar  $2 \mu\text{m}$ . Calibration bar in  $\text{ng mm}^{-2}$ .

cells and determining their Os content by ICP-MS. This increased from  $(4 \pm 1)$  to  $(49 \pm 7)$  ng Os per milligram protein when the treatment dose was increased from  $0.16 \mu\text{M}$  to  $1 \mu\text{M}$  **1** (Figure S10), whereas no Os was found in the mitochondria of untreated cells.

Additionally, SXRFN mapping showed that treatment of A2780 cells with **1** leads to significant perturbations in the cellular localization of bound Ca (Figures 2 and 3 and Figure S5). Calcium in cells is stored in the endoplasmic reticulum (ER). Intracellular levels of “free” Ca are normally very low (ca. 100 nM) and mobilization of stored  $\text{Ca}^{2+}$  is a signalling event leading to allosteric regulation of proteins and enzymes. High levels of cytoplasmic  $\text{Ca}^{2+}$  can stimulate mitochondrial activity and play a key role in apoptosis (programmed cell death), by activating the caspase chain after mitochondrial overload, as well as other types of cell death processes such as necrosis or autophagy.<sup>[15]</sup>

Free  $\text{Ca}^{2+}$  normally leaks out of cells after fixation, so only Ca chelated by proteins or other biomolecules can be detected. Our elemental maps show that bound Ca is concentrated in the nucleus in untreated A2780 cells, as it correlates well with Zn and P (Figure S5 in the Supporting Information). However, upon treatment of cells with  $1 \mu\text{M}$  of **1** we detect only extranuclear Ca, which is spread over the cytoplasm. Furthermore, Zn maps and TEM images show dramatic fragmentation of the nucleus and membrane blebbing (Figures 2 and 3 and Figure S9). Interestingly, cell-cycle analysis of A2780 treated with  $1 \mu\text{M}$  **1**, shows S-G2/M arrest and abnormally high sub-G0 populations (Figure S11), but Ca is not found in areas with a high density of Os, suggesting that mitochondrial loading with Ca might have not occurred (at least not after 24 h; Figure 4 and Figure S12, highlighted areas).

Complex **1** is relatively inert in chemical reactions but appears to be activated by glutathione in cancer cells resulting in initial formation of the hydroxido complex and loss of the iodido ligand, which is rapidly pumped out (Figure 5).<sup>[16]</sup> Both the intact complex and hydroxido metabolite are lipophilic cations, species often readily taken up by mitochondria.<sup>[17]</sup> We have observed rapid bursts of reactive oxygen species (ROS) and especially superoxide on treatment of cancer cells with **1**.<sup>[18]</sup> Proteins in the inner membrane of mitochondria are

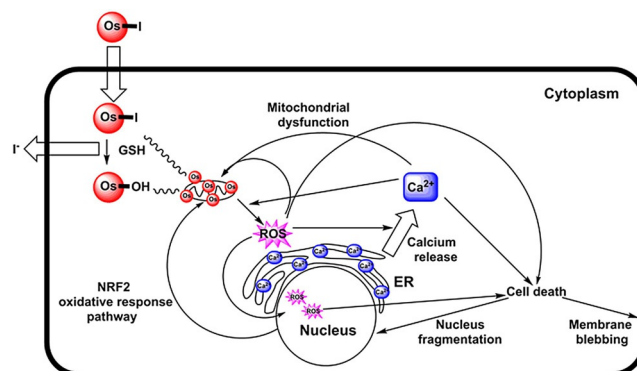


**Figure 5.** Possible pathways that link intracellular activation of **1** with Ca mobilization, mitochondrial dysfunction, ROS generation, and cell death.

active in electron transport and oxidative phosphorylation and are rich sources of ROS. Moreover, when GSH (an antioxidant) in cancer cells is depleted by L-buthionine sulfoximine (L-BSO), the activity of **1** is enhanced several-fold.<sup>[17]</sup> Additionally, Ca homeostasis is controlled by cellular levels of ROS, and high levels of radicals can induce the release of Ca from the ER to the cytoplasm.<sup>[19]</sup>

Complex **1** is approximately  $49\times$  more active than cisplatin over a range of 809 cancer cell lines. RNA sequencing and proteomic analysis of A2780 cells treated with **1** have shown a dramatic effect on the transcription of the mitochondrial chromosome indicative of mitochondrial dysfunction, together with a fast cellular response involving a mitochondria-linked oxidative stress response pathway (NRF2), and downregulation of key genes, consistent with ROS production and reduction in the ability of cells to respond.<sup>[3b]</sup> The ability of **1** to induce the release of bound Ca from the nucleus to the cytoplasm, and cause nuclear fragmentation as well as membrane blebbing can all be related to mitochondrial damage. Mitochondrial targeting offers a promising new strategy for the design of anti-cancer complexes. The mitochondria of cancer cells are known to be defective compared to the mitochondria of normal cells. Indeed we have detected three mutations in the mitochondrial DNA of A2780 human ovarian cells, all located in complex **1** (NADH dehydrogenase) of the electron transport chain.<sup>[3b]</sup> This difference between normal cells and cancer cells should provide a basis for selective drug activity towards cancer cells and reduce unwanted side-effects.

These experiments show that with recent advances in the design of synchrotron X-ray fluorescence nanoprobe it is now possible to map the distribution of metallodrugs in small organelles in cancer cells at pharmacologically relevant concentrations, down to nanomolar Os concentrations. This demonstration of mitochondrial targeting in ovarian cancer cells, together with our previous molecular cellular studies,<sup>[3b]</sup> show that complex **1** has an unusual mode of action.

## Experimental Section

XRF experiments were performed on the ID16A beamline at the ESRF synchrotron light source. Irradiation of the samples was done



at 17.05 keV energy and detection was performed using a pair of 6-element silicon drift diode detectors (Sensortech, UK). Scan step size was fixed at  $400 \times 400 \text{ nm}^2$  (dwell time 100 ms) for coarse scans and  $50 \times 50 \text{ nm}^2$  (dwell time 50 ms) for fine scans (although a sample was also measured using scan step size of  $20 \times 20 \text{ nm}^2$ ). Spectra were fitted using the free PyMCA software.<sup>[20]</sup> Due to overlap between Zn- $\alpha$  and Os- $\alpha_1$  emissions, fitting of Zn- $\beta$  emission and deconvolution of the signals were also used to provide quantitative data (Figure S2). The fitting procedure includes an attenuation correction that is significant for low Z elements such as P. It assumes a sample matrix consisting of 500 nm thick EPON. The quantitative calibration was determined using a thin film X-ray fluorescence 7-element reference sample (AXO Dresden GmbH, Table S2). The Supporting Information contains details of materials used, cell culture and preparation for TEM (Figure S9), X-ray phase-contrast (Figure S3), and XRF (spectrum Figure S2; further elemental maps Figures S1, S4, S5, S11 and S12), Os uptake (Table S1), size distribution of Os regions-of-interest (ROIs) (Figure S8), mitochondrial uptake (Figure S10), cycle analysis (Figure S11), fluorescence calibration data (Table S2), and image analysis (Figures S6 and S7).

## Acknowledgements

The XRF experiments were performed in the frame of ESRF proposals CH-4283 and CH-4546. We thank the ERC (Grant No. 247450), EPSRC (Grant No. EP/F034210/1), CRUK (Grant No. C53561/A19933) and Wellcome Trust (Grant No. 107691/Z/15/Z) for support, and members of EC COST Action CM1105 for stimulating discussions.

**Keywords:** bioinorganic chemistry • elemental mapping • metallodrugs • organometallic complexes • X-ray fluorescence

- [1] L. Kelland, *Nat. Rev. Cancer* **2007**, *7*, 573–584.
- [2] a) T. C. Johnstone, K. Suntharalingam, S. J. Lippard, *Philos. Trans. R. Soc. A* **2015**, *373*, 20140185; b) M. Hanif, M. V. Babak, C. G. Hartinger, *Drug Discovery Today* **2014**, *19*, 1640–1648.
- [3] a) Y. Fu, A. Habtemariam, A. M. Pizarro, S. H. van Rijt, D. J. Healey, P. A. Cooper, S. D. Shnyder, G. J. Clarkson, P. J. Sadler, *J. Med. Chem.* **2010**, *53*, 8192–8196; b) J. M. Hearn, I. Romero-Canelón, A. F. Munro, Y. Fu, A. M. Pizarro, M. J. Garnett, U. McDermott, N. O. Carragher, P. J. Sadler, *Proc. Natl. Acad. Sci. USA* **2015**, *112*, E3800–E3805.
- [4] a) L. E. Wedlock, M. R. Kilburn, R. Liu, J. A. Shaw, S. J. Berners-Price, N. P. Farrell, *Chem. Commun.* **2013**, *49*, 6944–6946; b) A. A. Legin, A. Schintlmeister, M. A. Jakupcic, M. Galanski, I. Lichtscheidl, M. Wagner, B. K. Keppler, *Chem. Sci.* **2014**, *5*, 3135–3143.
- [5] R. F. S. Lee, S. Escrig, M. Croisier, S. Clerc-Rosset, G. W. Knott, A. Meibom, C. A. Davey, K. Johnsson, P. J. Dyson, *Chem. Commun.* **2015**, *51*, 16486–16489.
- [6] L. E. Wedlock, M. R. Kilburn, J. B. Cliff, L. Filgueira, M. Saunders, S. J. Berners-Price, *Metalloomics* **2011**, *3*, 917–925.
- [7] P. Hoppe, S. Cohen, A. Meibom, *Geostand. Geoanal. Res.* **2013**, *37*, 111–154.
- [8] a) A. A. Hummer, A. Rompel, *Metalloomics* **2013**, *5*, 597–614; b) M. Shimura, A. Saito, S. Matsuyama, T. Sakuma, Y. Terui, K. Ueno, H. Yumoto, K. Yamauchi, K. Yamamura, H. Mimura, Y. Sano, M. Yabashi, K. Tamasaku, K. Nishio, Y. Nishino, K. Endo, K. Hatake, Y. Mori, Y. Ishizaka, T. Ishikawa, *Cancer Res.* **2005**, *65*, 4998–5002; c) K. J. Davis, J. A. Carrall, B. Lai, J. R. Aldrich-Wright, S. F. Ralph, C. T. Dillon, *Dalton Trans.* **2012**, *41*, 9417–9426; d) M. D. Hall, C. T. Dillon, M. Zhang, P. Beale, Z. Cai, B. Lai, A. J. Stampfl, T. W. Hambley, *J. Biol. Inorg. Chem.* **2003**, *8*, 726–732; e) M. D. Hall, R. A. Alderden, M. Zhang, P. J. Beale, Z. Cai, B. Lai, A. J. Stampfl, T. W. Hambley, *J. Struct. Biol.* **2006**, *155*, 38–44; f) S. Antony, J. B. Aitken, S. Vogt, B. Lai, T. Brown, L. Spiccia, H. H. Harris, *J. Biol. Inorg. Chem.* **2013**, *18*, 845–853; g) J. B. Aitken, S. Antony, C. M. Weekley, B. Lai, L. Spiccia, H. H. Harris, *Metalloomics* **2012**, *4*, 1051–1056; h) D. E. Morrison, J. B. Aitken, M. D. de Jonge, J. A. Ioppolo, H. H. Harris, L. M. Rendina, *Chem. Commun.* **2014**, *50*, 2252–2254; i) E. L. Crossley, J. B. Aitken, S. Vogt, H. H. Harris, L. M. Rendina, *Angew. Chem. Int. Ed.* **2010**, *49*, 1231–1233; *Angew. Chem.* **2010**, *122*, 1253–1255; j) J. B. Aitken, P. A. Lay, T. T. Hong Duong, R. Aran, P. K. Witting, H. H. Harris, B. Lai, S. Vogt, G. I. Giles, *J. Biol. Inorg. Chem.* **2012**, *17*, 589–598; k) K. L. Munro, A. Mariana, A. I. Klaving, A. J. Foster, B. Lai, S. Vogt, Z. Cai, H. H. Harris, C. T. Dillon, *Chem. Res. Toxicol.* **2008**, *21*, 1760–1769; l) L. E. Wu, A. Levina, H. H. Harris, Z. Cai, B. Lai, S. Vogt, D. E. James, P. A. Lay, *Angew. Chem. Int. Ed.* **2016**, *55*, 1742–1745; *Angew. Chem.* **2016**, *128*, 1774–1777.
- [9] J. B. Waern, H. H. Harries, B. Lai, Z. Cai, M. M. Harding, C. T. Dillon, *J. Biol. Inorg. Chem.* **2005**, *10*, 443–452.
- [10] a) F. Dubar, S. Bohic, C. Slomianny, J.-C. Morin, P. Thomas, H. Kalamou, Y. Guerardel, P. Cloetens, J. Khalife, C. Biot, *Chem. Commun.* **2012**, *48*, 910–912; b) E. L. Que, R. Bleher, F. E. Duncan, B. Y. Kong, S. C. Gleber, S. Vogt, S. A. Garwin, A. R. Bayer, V. P. Dravid, R. K. Woodruff, T. V. O'Halloran, *Nat. Chem.* **2014**, *7*, 130–139; c) S. Matsuyama, M. Shimura, H. Mimura, M. Fujii, H. Yumoto, Y. Sano, M. Yabashi, Y. Nishino, K. Tamasaku, T. Ishikawa, K. Yamauchi, *X-Ray Spectrom.* **2009**, *38*, 89–94; d) S. Gil, A. Carmona, G. Martinez-Criado, A. Leon, Y. Prezado, M. Sabes, *Biol. Trace Elem. Res.* **2015**, *163*, 177–183; e) B. Laforce, C. Carlier, B. Veke-mans, J. Villanova, R. Tucoulou, W. Ceelen, L. Vincze, *Sci. Rep.* **2016**, *6*, 29999; f) A. Carmona, P. Cloetens, G. Deves, S. Bohic, R. Ortega, *J. Anal. At. Spectrom.* **2008**, *23*, 1083; g) R. Ortega, P. Cloetens, G. Deves, A. Carmona, S. Bohic, *PLoS ONE* **2007**, *2*, e925; h) S. Chen, J. Deng, Y. Yuan, C. Flachenecker, R. Mak, B. Hornberger, Q. Jin, D. Shu, B. Lai, J. Maser, C. Roehrig, T. Paunesku, S. C. Gleber, D. J. Vine, L. Finney, J. VonOsinski, M. Bolbat, I. Spink, Z. Chen, J. Steele, D. Trapp, J. Irwin, M. Feser, E. Snyder, K. Brister, C. Jacobsen, G. Woloschak, S. Vogt, *J. Synchrotron Radiat.* **2014**, *21*, 66–75.
- [11] <http://www.esrf.eu/UsersAndScience/Experiments/XNP/ID16A>.
- [12] Q. Jin, T. Paunesku, B. Lai, S.-C. Gleber, S. Chen, L. Finney, D. Vine, S. Vogt, G. Woloschak, C. Jacobsen, *J. Microsc.* **2017**, *265*, 81–93.
- [13] R. McRae, B. Lai, C. J. Fahrni, *Metalloomics* **2013**, *5*, 52–61.
- [14] R. McRae, B. Lai, S. Vogt, C. J. Fahrni, *J. Struct. Biol.* **2006**, *155*, 22–29.
- [15] a) R. Rizzuto, C. Giorgi, A. Romagnoli, P. Pinton, *Curr. Mol. Med.* **2008**, *8*, 119–130; b) G. S. B. Williams, L. Boyman, A. C. Chikando, R. J. Khairallah, W. J. Lederer, *Proc. Natl. Acad. Sci. USA* **2013**, *110*, 10479–10486.
- [16] R. J. Needham, C. Sanchez-Cano, X. Zhang, I. Romero-Canelon, A. Habtemariam, M. S. Cooper, L. Meszaros, G. J. Clarkson, P. J. Blower, P. J. Sadler, *Angew. Chem. Int. Ed.* **2017**, *56*, 1017–1020; *Angew. Chem.* **2017**, *129*, 1037–1040.
- [17] M. P. Murphy, R. A. J. Smith, *Annu. Rev. Pharmacol. Toxicol.* **2007**, *47*, 629–656.
- [18] I. Romero-Canelón, M. Mos, P. J. Sadler, *J. Med. Chem.* **2015**, *58*, 7874–7880.
- [19] a) G. Ermak, K. J. A. Davies, *Mol. Immunol.* **2002**, *38*, 713–721; b) R. F. Feissner, J. Skalska, W. E. Gaum, S.-S. Sheu, *Front. Biosci.* **2009**, *14*, 1197–1218; c) A. Görlach, K. Bertram, S. Hudecova, O. Krizanov, *Redox Biol.* **2015**, *6*, 260–271.
- [20] V. A. Solé, E. Papillon, M. Cotte, P. Walter, J. Susini, *Spectrochim. Acta Part B* **2007**, *62*, 63–68.

Manuscript received: December 19, 2016

Revised: December 23, 2016

Accepted Article published: December 24, 2016

Final Article published: January 26, 2017